

Article

Carbon Supported Oxide-Rich Pd-Cu Bimetallic Electrocatalysts for Ethanol Electrooxidation in Alkaline Media Enhanced by Cu/CuO_x

Zengfeng Guo, Tengfei Liu, Wenpeng Li *, Cai Zhang, Dong Zhang and Zongjie Pang

Institute of Advanced Energy Materials and Chemistry, Key Lab of Fine Chemicals in Universities of Shandong, School of Chemistry and Pharmaceutical Engineering, Qilu University of Technology, Daxue Road, Changqing District, Jinan 250353, China; 18753197672@163.com (Z.G.); 15064048260@163.com (T.L.); zc_work@126.com (C.Z.); loudsilence@163.com (D.Z.); pangzj123@163.com (Z.P.)

* Correspondence: liwenpeng@qlu.edu.cn or wenpengli75@163.com; Tel.: +86-531-8963-1208

Academic Editor: Frédéric Jaouen

Received: 20 March 2016; Accepted: 19 April 2016; Published: 26 April 2016

Abstract: Different proportions of oxide-rich PdCu/C nanoparticle catalysts were prepared by the NaBH₄ reduction method, and their compositions were tuned by the molar ratios of the metal precursors. Among them, oxide-rich Pd_{0.9}Cu_{0.1}/C (Pd:Cu = 9:1, metal atomic ratio) exhibits the highest electrocatalytic activity for ethanol oxidation reaction (EOR) in alkaline media. X-ray photoelectron spectroscopy (XPS) and high resolution transmission electron microscopy (HRTEM) confirmed the existence of both Cu and CuO_x in the as-prepared Pd_{0.9}Cu_{0.1}/C. About 74% of the Cu atoms are in their oxide form (CuO or Cu₂O). Besides the synergistic effect of Cu, CuO_x existed in the Pd-Cu bimetallic nanoparticles works as a promoter for the EOR. The decreased Pd 3d electron density disclosed by XPS is ascribed to the formation of CuO_x and the spill-over of oxygen-containing species from CuO_x to Pd. The low Pd 3d electron density will decrease the adsorption of CH₃CO_{ads} intermediates. As a result, the electrocatalytic activity is enhanced. The onset potential of oxide-rich Pd_{0.9}Cu_{0.1}/C is negative shifted 150 mV compared to Pd/C. The oxide-rich Pd_{0.9}Cu_{0.1}/C also exhibited high stability, which indicated that it is a candidate for the anode of direct ethanol fuel cells (DEFCs).

Keywords: Pd-Cu alloy; Cu/CuO_x; fuel cells; ethanol oxidation reaction; oxides

1. Introduction

Fuel cell is a device of translating the chemical energy into electrical energy [1]. Hydrogen fueled proton exchange membrane fuel cells have attracted widespread attention, owing to their high energy conversion efficiency and low or zero emissions [2]. However, the production, storage and distribution of hydrogen are facing huge technical challenges [3]. The storage or transportation of methanol and ethanol are easier than that of hydrogen. Although the methanol fuel cells are expected to replace batteries as portable power sources [4], there are still some severe obstacles unsolved, such as methanol toxicity and the fuel crossover problem in Nafion based membranes [5]. In contrast, direct ethanol fuel cells (DEFCs) are considered as possible power source for electric vehicles and portable applications, due to their high efficiency, high energy density and low operating temperature [6]. Ethanol is non-toxic [7]. It is an interesting alternative renewable fuel, which can be produced in large quantity from the fermentation process. Moreover, the penetration efficiency of ethanol through the Nafion membrane is much lower than that of methanol [4].

Pt-based catalysts are most widely used for ethanol oxidation reaction (EOR) in acidic media, e.g., Pt [8,9], Pt-Rh [10], Pt-Ir [11], and so on. The history of using platinum as anode for EOR can be traced back to 1940s [12]. However, Pt-based catalysts are easily poisoned in acid medium

by ethanol dissociation intermediate species particularly CO-like intermediates [13]. Platinum is rare and expensive, which hinders its wide application in ethanol fuel cells [14–16]. In recent years, the electrocatalysts for alcohol oxidation operating in alkaline electrolytes have attracted great interests [17]. In alkaline media, kinetics of alcohol oxidation process are significantly increased and corrosion is decreased [18,19]. Furthermore, the selectivity for ethanol electro-oxidation to CO_2 could be improved significantly in alkaline media [20].

Palladium is known to be a good electrocatalyst for ethanol oxidation in alkaline solution [21,22], and it is at least fifty times more abundant than Pt on earth [23]. However, the activity and durability of Pd catalyst are urgent to improve because of the rapid deactivation of the catalyst [13]. Alloying Pd with other elements based on d-band theory [24] is a common method to improve the activity and stability. Successful examples of Pd-alloy electrocatalysts include but not limit to Pd-Au [25], Pd-Ni [26], Pd-Co [27], Pd-Ag [28], Pd-Cu [29], Pd-Ni-P [30], and so on. Stoichiometry of the electrocatalysts is of great significance to improve the catalytic activity [31]. Meanwhile, oxides also affect the electrocatalytic performance of Pd-based electrocatalysts for EOR. Transition metal oxides such as Co_3O_4 , SnO_2 , CeO_2 and NiO [18,32] have been used as promoters to improve the electrocatalytic performance. In summary, both the second metals and the metal-oxides can be used to promote the electrocatalytic activity of Pd-based catalysts for EOR. Naturally a question appears: Can the combination of the second metal and its coexisted oxides improve the electrocatalytic performance in EOR better? We examined the related references, and noticed an interesting example about Pd-Ni system. The Ni catalyst for methanol oxidation has been reported since 2004 [33], and Pd-Ni for EOR was reported in 2010 [26]. However, the energy efficient role of Ni/NiO in Pd-Ni catalysts has not been discussed until the report published in 2014 [32]. This enlightened us to focus on the new oxide-rich Pd-M systems (M: second metal) and the role of M/MO_x .

Recently, Pd-Cu system has been discovered by former studies to have optimal electroactivity [34–38]. More and more reports about Pd-Cu system for EOR appeared [4,29,31,39–46] and the synergistic effect of Cu has been confirmed. A preliminary comparison of some Pd-Cu electrocatalysts is provided in Table 1. As is well known, Cu is easily oxidized by the ambient air [47,48]. CuO and Cu_2O have aroused much attention in many research fields such as lithium-ion batteries [49–51], photoelectrocatalytic processes [52–54], electrochromic devices [55,56], supercapacitors [57–59], dye-sensitized solar cells [60,61], gas sensors [62,63], non-enzymatic amperometric sensors of glucose and hydrogen peroxide [64–66], and so on. CuO has been used as the electrocatalyst for the oxidation reactions concerned with nitrite, hydrazine, water, glucose and ascorbic acid [67–71]. Cu_2O has been used as the electrocatalyst for oxygen reduction reaction and glucose oxidation reaction [72,73]. When we start this work, there is no report about CuO or Cu_2O used as the promoter for EOR. After we had started the research, a paper by Rostami and his coworkers appeared that reported that Cu_2O promotes the EOR at Pd [74]. Compared with Pd loaded on multi-walled carbon nanotube (Pd/MWCNT), the onset potential of Pd/ Cu_2O /MWCNT shifted toward negative value by 120 mV. In this paper, carbon supported oxide-rich Pd-Cu bimetallic electrocatalysts containing both Cu and its oxides are prepared under mild conditions. Compared to Pd/C, the onset potential of oxide-rich $\text{Pd}_{0.9}\text{Cu}_{0.1}/\text{C}$ (Pd:Cu = 9:1, metal atomic ratio) is negative shifted 150 mV. The negative shift of onset potential indicates a higher catalytic activity. Though either the synergy of Cu or the promotion of Cu_2O alone for the EOR at Pd has been reported, the catalysts enhanced by the combination of Cu and CuO_x have not been reported. Compared with Pd, the shift of oxide-rich $\text{Pd}_{0.9}\text{Cu}_{0.1}$ (150 mV) for EOR is more negative than almost all the Pd-Cu electrocatalysts mentioned above (Table 1) and the Pd/ Cu_2O [74], which indicates that the combination of Cu/ CuO_x also exhibits excellent promoting effect.

Table 1. Comparison of electrocatalytic performance of the Pd-Cu system with Pd for ethanol oxidation reaction (EOR).

Catalysts	Negative Shift	Morphology	Support	Ref.
Pd-on-Cu ¹	35 mV	Pd-on-Cu nanocrystals	reduced graphene oxide	[4]
Pd-Cu	-	ultrafine nanoporous Cu-Pd alloys	carbon	[29]
Pd-Cu ²	15 mV	Pd-Cu alloy nanoparticles	carbon	[31]
Pd/Cu ²	138 mV	bimetallic nanoparticles	graphene nanosheets	[39]
Pd-Cu	-	Pd-Cu nanoparticles	reduced graphene oxide	[40]
Pd-Cu ²	55 mV	Pd-Cu nanoparticles	carbon	[41]
Pd-Cu ²	63 mV	Pd _x Cu _{100-x} networks	no support	[42]
Pd-Cu ²	79 mV	surface palladium rich Cu _x Pd _y	carbon	[43]
Pd-Cu ³	38 mV	Pd-Cu alloying	carbon nanotubes	[44]
Pd-Cu ²	30 mV	3D nanochain network Pd-Cu alloy	no support	[45]
Pd-Cu ²	88 mV	monodisperse Pd-Cu bimetallic nanocrystals	no support	[46]

¹: Compare with Pd/reduced-graphene-oxide; ²: Compare with Pd/C; ³: Compare with Pd/carbon-nanotubes.

2. Results and Discussion

2.1. Materials Characterization

The X-ray diffraction (XRD) patterns for the as-synthesized Pd/C, oxide-rich Pd_{0.6}Cu_{0.4}/C, oxide-rich Pd_{0.7}Cu_{0.3}/C, oxide-rich Pd_{0.8}Cu_{0.2}/C, oxide-rich Pd_{0.9}Cu_{0.1}/C and oxide-rich Pd_{0.95}Cu_{0.05}/C catalysts are shown in Figure 1. There are four typical diffraction peaks on the XRD diffractograms. The peak located at about 25° is associated with the Vulcan XC-72 carbon (002) lattice plane. The other three peaks around 40°, 46° and 68° are characteristic of face centered cubic (fcc) crystalline Pd, corresponding to the diffraction peaks of Pd crystal faces (111), (200) and (220), respectively. The XRD patterns do not show any peak corresponding to the Cu [75], CuO [49] or Cu₂O [58]. These indicated that Cu(0), CuO and Cu₂O have not existed in the form of crystals as the other studies described [29,39]. All the diffraction peaks of the oxide-rich PdCu/C catalysts shift toward higher 2θ values compared with the corresponding reflection of Pd/C catalyst. The shifts of the diffraction peaks were caused by the difference in size between Pd and Cu, which further indicated that Cu atoms have entered into the Pd lattice and formed Pd-Cu alloy [76]. The size of the catalyst particles can be estimated according to Scherrer's equation [77]. The calculated average particle sizes of Pd/C, oxide-rich Pd_{0.6}Cu_{0.4}/C, oxide-rich Pd_{0.7}Cu_{0.3}/C, oxide-rich Pd_{0.8}Cu_{0.2}/C, oxide-rich Pd_{0.9}Cu_{0.1}/C, and oxide-rich Pd_{0.95}Cu_{0.05}/C are 5.5, 5.3, 5.1, 4.9, 4.5, and 4.8 nm, respectively. The size of oxide-rich PdCu/C nanoparticles is smaller than that of Pd/C.

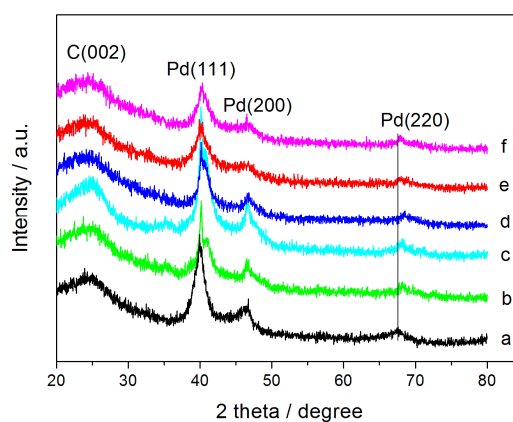


Figure 1. The X-ray diffraction (XRD) patterns of: Pd/C (a); oxide-rich Pd_{0.6}Cu_{0.4}/C (b); oxide-rich Pd_{0.7}Cu_{0.3}/C (c); oxide-rich Pd_{0.8}Cu_{0.2}/C (d); oxide-rich Pd_{0.9}Cu_{0.1}/C (e); and oxide-rich Pd_{0.95}Cu_{0.05}/C (f).

The transmission electron microscopy (TEM) patterns and particle size distribution histograms of the Pd/C and oxide-rich Pd_{0.9}Cu_{0.1}/C catalysts were shown in Figure 2. Oxide-rich Pd_{0.9}Cu_{0.1}/C was chosen as the representative because it exhibits the best performance for the anode oxidation of ethanol, which will be discussed later. The average diameters of the Pd/C and oxide-rich Pd_{0.9}Cu_{0.1}/C catalysts observed by TEM images are 5.5 and 4.5 nm, respectively. Furthermore, the high resolution transmission electron microscopy (HRTEM) patterns of oxide-rich Pd_{0.9}Cu_{0.1}/C catalyst (Figure 3a) show well-resolved fringes with spacing of 0.223 and 0.193 nm, which are ascribed to the (111), (200) planes of Pd crystal, respectively. Most of the oxide-rich Pd_{0.9}Cu_{0.1} nanoparticles are in the size of less than 8 nm (Figure 2d). We did not find any diffraction fringes corresponding to Cu or CuO in the nanoparticles with the size less than 8 nm, which is consistent with the result of XRD. In rarely appearing large Pd-Cu nanoparticles (with the size of ~10 nm), we found the CuO diffraction fringes of CuO (002) plane with spacing of 0.254 nm [57] (Figure 3b). This provides visible evidence of the coexisting CuO_x in Pd-Cu system.

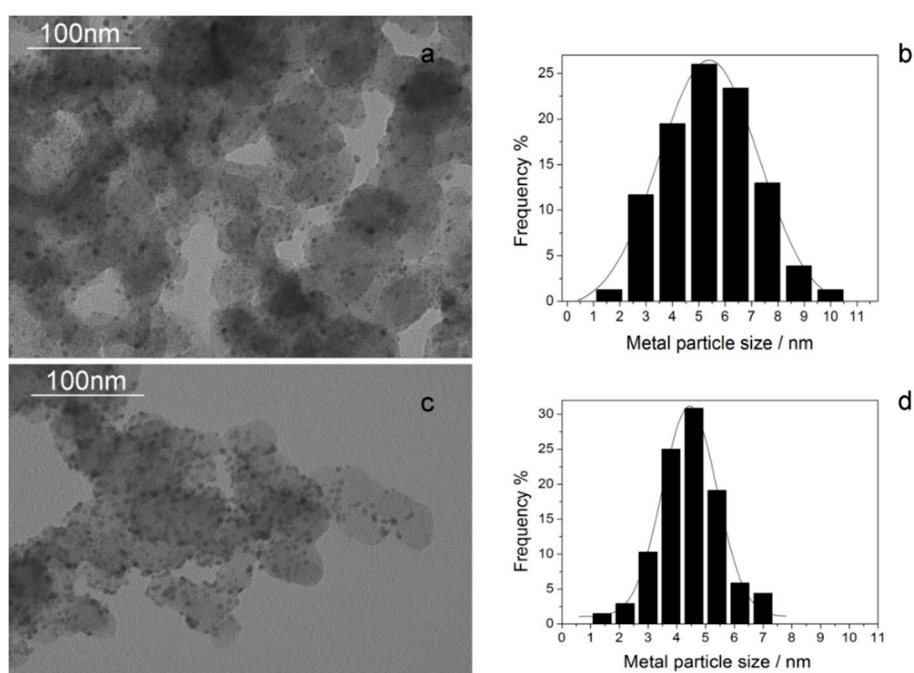


Figure 2. The transmission electron microscopy (TEM) patterns and particle size distribution histograms of: Pd/C (a,b) and oxide-rich Pd_{0.9}Cu_{0.1}/C (c,d).

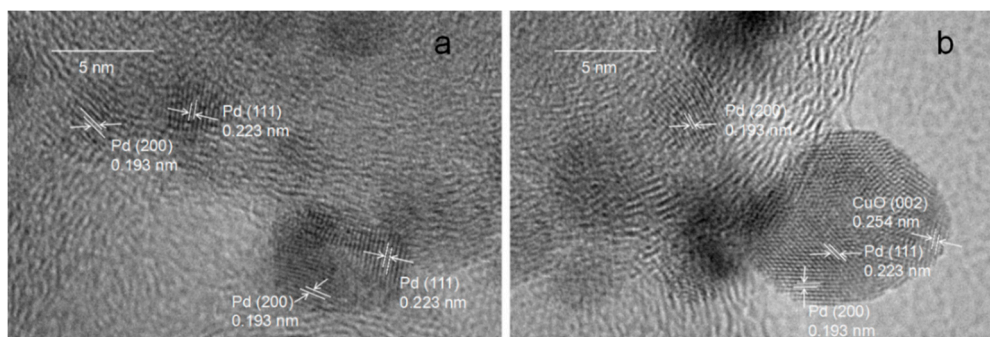


Figure 3. The high resolution transmission electron microscopy (HRTEM) patterns of oxide-rich Pd_{0.9}Cu_{0.1}/C (a,b).

The X-ray photoelectron spectroscopy (XPS) [78,79] was used to further explore the chemical states and surface compositions of Pd/C and oxide-rich Pd_{0.9}Cu_{0.1}/C catalysts (Figure 4). All the XPS curves are fitted by the Gaussian–Lorentzian (20% Gaussian) method after background subtraction using Shirley’s method [80]. Figure 4a is composed of Pd 3d signal. For Pd/C catalyst, the peaks of the Pd 3d_{5/2} and Pd 3d_{3/2} (deconvoluted into Pd and PdO_y (0 < y < 2) [81]) are located at 336.0 and 341.1 eV, respectively. The Pd 3d_{5/2} and Pd 3d_{3/2} binding energy values of oxide-rich Pd_{0.9}Cu_{0.1}/C shift by +0.2 eV. In the Cu 2p range (Figure 4b), the peak at 932.1 eV corresponds to zero-valent copper, while the peaks at 933.1 and 934.6 eV correspond to the Cu₂O and CuO, respectively. The compositions of the as-prepared catalysts determined by XPS are displayed in Table 2. The metal atomic ratio (Pd:Cu) of oxide-rich Pd_{0.9}Cu_{0.1}/C catalyst calculated from XPS spectra is Pd_{0.92}Cu_{0.08}, which is similar with that of the metal precursor. PdO has been reported to be a good catalyst for EOR [82]. The coexisted CuO and Cu₂O are helpful for the formation of oxygen containing species (OH[−]_{ads}) [31]. OH[−]_{ads} can react with acetaldehyde and CO-type intermediate species, thus the active sites on Pd surface can be released [83], which will benefit for the ethanol oxidation. The positive shift of the Pd 3d binding energy indicates that the Pd 3d electron density is decreased. This positive shift is quite different with the negative shifts reported in other references about Pd-based bimetallic catalysts such as Pd-Ni [84] and Pd-Co [85] electrocatalysts. Their negative shifts resulted from the slight electrons transfer from Ni to Pd or Co to Pd, consistent with their electronegativity. Though the electronegativity of Cu is also less than Pd, XPS analysis indicates that 74% of the copper atoms are in their oxide form (CuO or Cu₂O) (Table 2), thus the positive shift can be ascribed to the formation of CuO_x and the spill-over of oxygen-containing species from CuO_x to Pd. The positive shifts can also be found in the literature of Pd-Cu-Fe [86], Pd-P [87], and so on. The shift of binding energies results in a decrease of the intermediate adsorption energy [30,88], thus the active sites of Pd can be kept or be released. XPS is regarded to be a surface-analysis method [78]. In this paper, inductively coupled plasma-atomic emission spectrometer (ICP-AES) is used for the accurate determination of the bulk composition of the catalysts (Table 3).

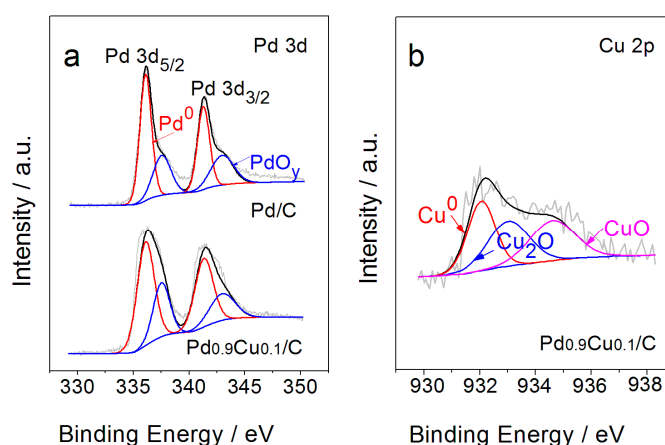


Figure 4. The X-ray photoelectron spectroscopy (XPS) patterns of: Pd/C (a); and oxide-rich Pd_{0.9}Cu_{0.1}/C (a,b).

Table 2. Compositions of Pd/C and oxide-rich Pd_{0.9}Cu_{0.1}/C (by X-ray photoelectron spectroscopy (XPS)).

Electrode	Pd:Cu	Pd:Cu:O	Metal Pd:Cu	Pd(0):Pd(II)	Cu(0):Cu(I):Cu(II)
Pd/C	Pd	Pd _{0.75} :O _{0.25}	Pd	Pd(0) _{0.66} :Pd(II) _{0.34}	-
Pd _{0.9} Cu _{0.1} /C	Pd _{0.92} :Cu _{0.08}	Pd _{0.68} :Cu _{0.06} :O _{0.26}	Pd _{0.96} :Cu _{0.04}	Pd(0) _{0.63} :Pd(II) _{0.37}	Cu(0) _{0.26} :Cu(I) _{0.49} :Cu(II) _{0.25}

Table 3. Activity of Pd/C and oxide-rich PdCu/C for EOR and compositions determined by inductively coupled plasma-atomic emission spectrometer (ICP-AES).

Electrode	Onset Potential (V)	1.0 M KOH + 1.0 M C ₂ H ₅ OH			Pd Cu Atomic Ratios by ICP-AES
		<i>I_f</i> (mA·mg ⁻¹ _{Pd})	<i>I_b</i> (mA·mg ⁻¹ _{Pd})	<i>I_f</i> / <i>I_b</i>	
Pd/C	-552.5 mV	114.51	287.74	0.40	Pd
Pd _{0.95} Cu _{0.05} /C	-621.2 mV	230.93	-	-	Pd _{0.94} Cu _{0.06}
Pd _{0.9} Cu _{0.1} /C	-704.8 mV	229.61	428.3	0.54	Pd _{0.90} Cu _{0.10}
Pd _{0.8} Cu _{0.2} /C	-618.7 mV	164.94	-	-	Pd _{0.81} Cu _{0.19}
Pd _{0.7} Cu _{0.3} /C	-600.7 mV	77.93	-	-	Pd _{0.71} Cu _{0.29}
Pd _{0.6} Cu _{0.4} /C	-586.9 mV	55.85	-	-	Pd _{0.61} Cu _{0.39}

2.2. Electrochemical Performance

It is generally accepted that the Pd-Cu alloy can boost catalytic activity for EOR compared to monometallic Pd or Cu catalyst. It can be seen from the polarization curves of ref. [89] that the onset potential of EOR at Cu electrode is about 0.47 V *vs.* Ag/AgCl. Obviously, the activity of Cu for EOR is much lower than that of Pd. Cu₂O does not exhibit electrocatalytic activity for EOR, though it can be used as a promoter [74]. In this paper, we focused on the Pd-Cu bimetallic catalysts. The cyclic voltammograms (CVs) of Pd/C, oxide-rich Pd_{0.6}Cu_{0.4}/C, oxide-rich Pd_{0.7}Cu_{0.3}/C, oxide-rich Pd_{0.8}Cu_{0.2}/C, oxide-rich Pd_{0.9}Cu_{0.1}/C and oxide-rich Pd_{0.95}Cu_{0.05}/C catalysts were measured in 1 M NaOH solution at a scan rate of 10 mV·s⁻¹ (shown in Figure 5). The shape of the CVs is the typical behavior of the Pd modified electrode in alkaline media [90]. The peaks (A₁, B₁) at the potential range from -0.8 to -0.5 V *versus* Hg/HgO are assigned to the desorption/adsorption of hydrogen [91]. The conspicuous peak (A₂) of the catalysts at -0.4 V is due to the absorption of OH⁻ on the electrocatalyst surface while those peaks (A₃, B₂) from -0.4 to 0.1V correspond to the oxidation of surface metal and the reduction of thus formed oxides [92]. The peaks (A₂) of the Pd/C, oxide-rich Pd_{0.6}Cu_{0.4}/C, oxide-rich Pd_{0.7}Cu_{0.3}/C, oxide-rich Pd_{0.8}Cu_{0.2}/C, oxide-rich Pd_{0.9}Cu_{0.1}/C and oxide-rich Pd_{0.95}Cu_{0.05}/C were at -0.42, -0.37, -0.40, -0.44, -0.47, and -0.45 V, respectively. In a former investigation, Dong and his coworkers [39] indicated that a negative shifted absorption peak of OH⁻ would give rise to a greater amount of OH⁻ and OH_{ads} species to react with CH₃CO_{ads} in ethanol electrooxidation process, which leads to higher electroactivity and better tolerance to intermediate species by refreshing surface active sites of Pd.

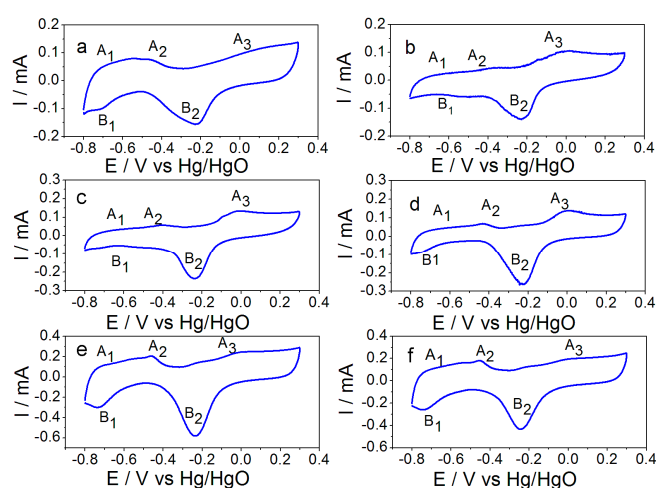


Figure 5. Cyclic voltammograms (CV) curves of: (a) Pd/C; (b) oxide-rich Pd_{0.6}Cu_{0.4}/C; (c) oxide-rich Pd_{0.7}Cu_{0.3}/C; (d) oxide-rich Pd_{0.8}Cu_{0.2}/C; (e) oxide-rich Pd_{0.9}Cu_{0.1}/C; and (f) oxide-rich Pd_{0.95}Cu_{0.05}/C in deaerated 1 M NaOH. Scan rate: 10 mV·s⁻¹. The peaks are corresponded to desorption of hydrogen (A₁), absorption of OH⁻ (A₂), oxidation of surface metal (A₃), adsorption of hydrogen (B₁) and reduction of formed oxides (B₂).

The linear sweep voltammetry (LSV) curves of the Pd/C and oxide-rich PdCu/C catalysts in 1.0 M NaOH and 1.0 M CH₃CH₂OH solution are shown in Figure 6. The peak in the forward scan corresponds to the anodic oxidation of ethanol. The forward anodic peak current densities (I_f) and the onset potential of the Pd/C and oxide-rich PdCu/C catalysts were shown in Table 3. The onset potential of the oxide-rich Pd_{0.95}Cu_{0.05}/C, oxide-rich Pd_{0.9}Cu_{0.1}/C, oxide-rich Pd_{0.8}Cu_{0.2}/C, oxide-rich Pd_{0.7}Cu_{0.3}/C, and oxide-rich Pd_{0.6}Cu_{0.4}/C catalysts are 68, 150, 66, 48 and 34 mV, respectively, more negative than that at the Pd/C catalyst electrode. The results demonstrate that oxide-rich Pd_{0.9}Cu_{0.1}/C exhibits the highest activity toward ethanol oxidation in terms of onset potential and peak-current density. As mentioned above, the onset potential of EOR at Pd/Cu₂O/MWCNT has a negative shift of 120 mV compared with Pd/MWCNT [74], and the onset potential at the Pd_{0.9}Cu_{0.1}/C has a negative shift of 15 mV compared with Pd/C [31]. Our oxide-rich Pd_{0.9}Cu_{0.1}/C exhibits a negative shift of 150 mV compared with Pd/C. XPS analysis indicates that there are Cu and CuO_x coexisted in the oxide-rich Pd_{0.9}Cu_{0.1} nanoparticles. Thus, we draw a conclusion that the combination of Cu/CuO_x greatly improves the EOR at Pd.

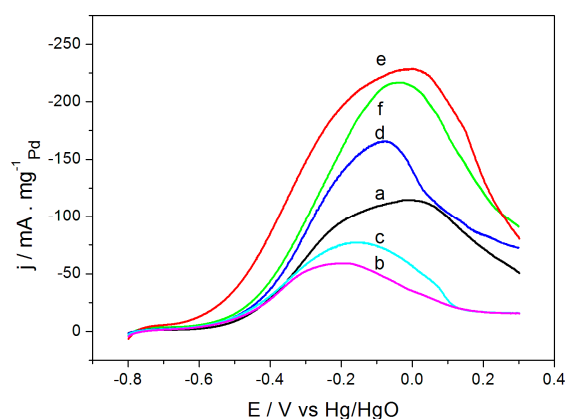


Figure 6. Linear sweep voltammetry (LSV) curves of: (a) Pd/C; (b) oxide-rich Pd_{0.6}Cu_{0.4}/C; (c) oxide-rich Pd_{0.7}Cu_{0.3}/C; (d) oxide-rich Pd_{0.8}Cu_{0.2}/C; (e) oxide-rich Pd_{0.9}Cu_{0.1}/C; and (f) oxide-rich Pd_{0.95}Cu_{0.05}/C in deaerated 1 M NaOH containing 1 M C₂H₅OH. Scan rate: 10 mV · s⁻¹.

Figure 7 displays the cyclic voltammograms (CV) of the Pd/C and oxide-rich Pd_{0.9}Cu_{0.1}/C catalysts in 1.0 M NaOH and 1.0 M CH₃CH₂OH solution. The peak in the forward scan corresponds to ethanol oxidation, while the peak in the reverse scan is mainly assigned to the removal of incompletely oxidized carbonaceous species rather than the oxidation of freshly chemisorbed species coming from ethanol adsorption [39]. The forward anodic peak current density (I_f) and the reverse anodic peak current density (I_b) of Pd/C and oxide-rich Pd_{0.9}Cu_{0.1}/C are shown in Table 3. The ratio (I_f/I_b) of Pd/C and oxide-rich Pd_{0.9}Cu_{0.1}/C are 0.40 and 0.54, respectively. The catalyst tolerance for intermediate carbonaceous species accumulated on the electrode surface in the reaction can be measured by the ratio of the forward anodic peak current density (I_f) to the reverse anodic peak current density (I_b) [93]. The higher ratio of oxide-rich Pd_{0.9}Cu_{0.1}/C implied that the ethanol was more completely oxidized and there was less carbonaceous residue accumulated on the electrode surface [39].

The electrochemical stability of Pd/C and oxide-rich Pd_{0.9}Cu_{0.1}/C catalysts for ethanol electro-oxidation was investigated by chronoamperometry in 1 M NaOH containing 1 M C₂H₅OH aqueous solution at -0.5 V for 3600 s (Figure 8) [90]. The initial currents drop quickly for both the oxide-rich Pd_{0.9}Cu_{0.1}/C and Pd/C catalysts, and then the current densities of the catalysts become relatively stable. The phenomenon is similar to the earlier report [4]. The current density at oxide-rich Pd_{0.9}Cu_{0.1}/C catalyst is higher than Pd/C catalyst with time in oxidation of ethanol, which indicates that the stability of the oxide-rich Pd_{0.9}Cu_{0.1}/C is better than that of Pd/C.

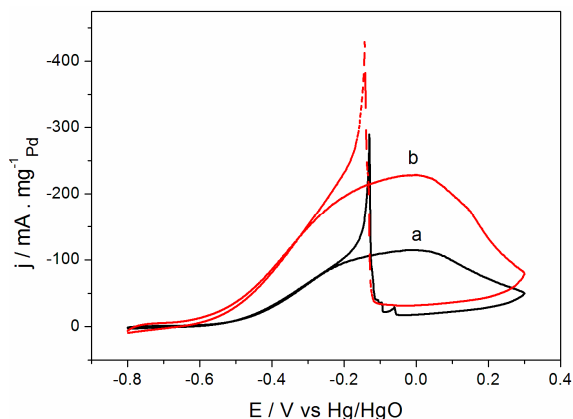


Figure 7. CV curves of: (a) Pd/C; and (b) oxide-rich Pd_{0.9}Cu_{0.1}/C in deaerated 1 M NaOH containing 1 M C₂H₅OH. Scan rate: 10 mV · s⁻¹.

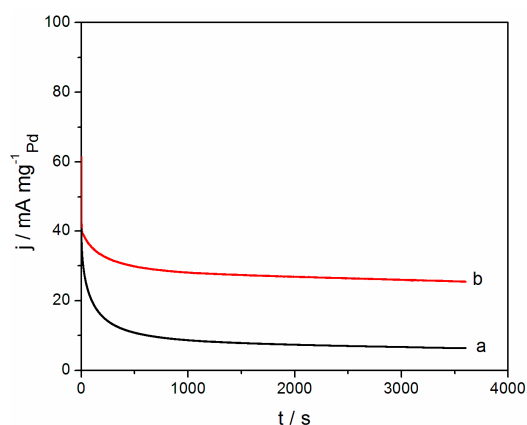


Figure 8. The chronoamperometric curves of (a) Pd/C and (b) oxide-rich Pd_{0.9}Cu_{0.1}/C in 1 M NaOH containing 1 M C₂H₅OH. Potential: -0.5 V vs. Hg/HgO.

3. Materials and Methods

3.1. Chemical Reagents

PdCl₂ was purchased from Sinopharm Chemical Reagent Co.Ltd (Shanghai, China). PdCl₂ was dissolved in a 0.2 M HCl solution before use. The Vulcan carbon powder XC-72R was obtained from Cabot Corporation (Cabot Corp., Billerica, MA, USA). Nafion solution (5%) was obtained from DuPont (Delaware, DE, USA). All other chemicals were of analytical grade and used as acquired unless otherwise noted. Triple-distilled water was used throughout.

3.2. Preparation of the Catalysts

The Pd/C and oxide-rich PdCu/C catalysts with the appropriate alloy composition and a metal loading of 20 wt% were prepared by chemical reduction with NaBH₄ as a reducing agent that we have used before [80,94]. Briefly, we prepared the carbon mixture with carbon black and triple-distilled water according to the proportion of 160 mg:100 mL and agitated under ultrasonication for 30 min. Then appropriate volume of 0.2 M PdCl₂ and 0.2 M CuSO₄ used as the precursors were added to the carbon suspension under stirring for 30 min. Next, 1 M NaOH solution was added to adjust the pH to 10 and 3 mL of 5 wt% freshly prepared sodium borohydride solution was added. The mixture was left to stand overnight after stirring for 15 min, and filtered in air at room temperature. The electrocatalysts were thoroughly washed with triple-distilled water to fully remove all residual reducing agents and salts. Finally, the products were dried in a vacuum oven at 403 K

for 6 h. The catalysts were stored in tubes with screw caps without further treatment. The air was not removed from the tubes. They were used as the Pd/C and oxide-rich PdCu/C in this paper. The final compositions of the oxide-rich PdCu/C electrocatalysts were adjusted by the molar ratios of the metal precursors.

3.3. Preparation of the Working Electrode

To prepare the catalysts modified working electrodes, an ink of the sample was prepared by dispersing 4 mg of the catalyst powder in a mixture of 0.2 mL water and 0.2 mL ethanol with ultrasonic stirring for 15 min. The glassy carbon electrode (GCE, 3 mm in diameter) was carefully polished with 0.05 μm alumina (Al_2O_3) powder, and washed with the triple-distilled water before use. Then, 10 μL ($2 \mu\text{L} \times 5$ times) of this ink was coated on the GCE and the ink was allowed to dry in air. 3 μL of Nafion solution (5 wt%) was added onto the GCE to fix the catalyst and dried at room temperature.

3.4. Materials Characterization

The metal phases and crystalline particle sizes of the products were obtained with a Bruker D8 advance X-ray diffractometer (Bruker AXS GmbH, Karlsruhe, Germany) operating at 40 keV and 30 mA with Cu $K\alpha$ radiation source, $\lambda = 0.15406$ nm. The morphology of the samples was characterized by TEM on a JEOL JEM-1011 (JEOL, Beijing, China). HRTEM was carried out on a JEOL JEM 2100 (JEOL, Beijing, China). The chemical states and surface compositions were determined by X-ray photoelectron spectroscopy. The X-ray photoelectron spectroscopy was obtained with an ESCALAB 250 (ThermoFisher SCIENTIFIC, Shanghai, China) spectrometer using Al $K\alpha$ (1486.71 eV) X-ray radiation for excitation. The accurate compositions were measured with an inductively coupled plasma-atomic emission spectrometer (Optima 2000DV, PERKINELMER, Massachusetts, MA, USA).

3.5. Electrochemical Measurements

The electrochemical measurements were performed with a CHI832B electrochemical workstation (CH Instruments, Austin, TX, USA) and a conventional three-electrode electrochemical cell. A carbon-rod was used as the auxiliary electrode, a GCE was used as working electrode, and Hg/HgO electrode was used as a reference electrode. All electrolyte solutions have been deaerated with N_2 for 30 min just before use. N_2 atmosphere was used throughout the electrochemical measurements. The electrochemical performance of Pd/C and oxide-rich PdCu/C catalysts was examined by cyclic voltammetry (CV), linear sweep voltammetry (LSV) and chronoamperometry methods. The CV curves of all catalysts were measured in 1 M NaOH solution, at a scan rate of $10 \text{ mV} \cdot \text{s}^{-1}$. The LSV curves of all catalysts were measured in a solution comprised of 1 M NaOH and 1 M $\text{C}_2\text{H}_5\text{OH}$, at a scan rate of $10 \text{ mV} \cdot \text{s}^{-1}$. The cyclic voltammograms curves of the Pd/C and oxide-rich $\text{Pd}_{0.9}\text{Cu}_{0.1}/\text{C}$ were measured in a solution comprised of 1 M NaOH and 1 M $\text{C}_2\text{H}_5\text{OH}$, at a scan rate of $10 \text{ mV} \cdot \text{s}^{-1}$. The chronoamperometric curves of the Pd/C and oxide-rich $\text{Pd}_{0.9}\text{Cu}_{0.1}/\text{C}$ catalysts were measured in the same solution comprised of 1 M NaOH and 1 M $\text{C}_2\text{H}_5\text{OH}$ at an applied potential of -0.5 V (*vs.* Hg/HgO) for 3600 s. All electrochemical tests were carried out at room temperature.

4. Conclusions

In summary, we prepared carbon loaded Pd-Cu bimetallic nanoparticles with the existence of Cu and its oxides (Cu_2O and CuO). The combination of Cu/ CuO_x greatly improves the electrocatalytic performance of Pd-Cu bimetallic system for ethanol electrooxidation. The oxide-rich $\text{Pd}_{0.9}\text{Cu}_{0.1}/\text{C}$ also exhibited high stability, which indicated that it is a candidate for the anode of direct ethanol fuel cells.

Acknowledgments: This work is supported by the Foundation of Science-Technology Development Plan of Jinan City (No. 201311035) and Program for Scientific research innovation team in Colleges and Universities of Shandong Province. The assistance of Huiling Liu and Baoyun Yu are gratefully acknowledged.

Author Contributions: The corresponding author Wenpeng Li is the advisor/director of all other authors. Wenpeng Li and Zengfeng Guo conceived and designed the experiments; Zengfeng Guo and Dong Zhang performed the experiments; Tengfei Liu and Cai Zhang analyzed the data; Zongjie Pang repeated the electrocatalytic experiments to make sure the results to be repeatable; Zengfeng Guo wrote the paper; and Tengfei Liu examined the revised paper.

Conflicts of Interest: The authors declare no conflict of interest.

References

1. Carrette, L.; Friedrich, K.A.; Stimming, U. Fuel cells: Principles, types, fuels, and applications. *ChemPhysChem* **2000**, *1*, 162–193. [[CrossRef](#)]
2. Vielstich, W.; Lamm, A.; Gasteiger, H.A. *Handbook of Fuel Cells: Fundamentals, Technology, Applications*; John Wiley & Sons Inc.: New York, NY, USA, 2003.
3. U.S. Department of Energy. *Basic Research Needs for the Hydrogen Economy*; U.S. Department of Energy: Washington, DC, USA, 2004.
4. Zhang, Q.L.; Zheng, J.N.; Xu, T.Q.; Wang, A.J.; Wei, J.; Chen, J.R.; Feng, J.J. Simple one-pot preparation of Pd-on-Cu nanocrystals supported on reduced graphene oxide for enhanced ethanol electrooxidation. *Electrochim. Acta* **2014**, *132*, 551–560. [[CrossRef](#)]
5. Yu, X.; Pickup, P.G. Recent advances in direct formic acid fuel cells (DFAFC). *J. Power Sources* **2008**, *182*, 124–132. [[CrossRef](#)]
6. Ribeiro, J.; dos Anjos, D.M.; Léger, J.M.; Hahn, F.; Olivi, P.; de Andrade, A.R.; Tremiliosi-Filho, G.; Kokoh, K.B. Effect of W on PtSn/C catalysts for ethanol electrooxidation. *J. Appl. Electrochem.* **2008**, *38*, 653–662. [[CrossRef](#)]
7. Song, S.; Wang, Y.; Shen, P. Thermodynamic and kinetic considerations for ethanol electrooxidation in direct ethanol fuel cells. *Chin. J. Catal.* **2007**, *28*, 752–754. [[CrossRef](#)]
8. Giz, M.J.; Camara, G.A. The ethanol electrooxidation reaction at Pt (111): The effect of ethanol concentration. *J. Electroanal. Chem.* **2009**, *625*, 117–122. [[CrossRef](#)]
9. Camara, G.A.; Iwasita, T. Parallel pathways of ethanol oxidation: The effect of ethanol concentration. *J. Electroanal. Chem.* **2005**, *578*, 315–321. [[CrossRef](#)]
10. Yuan, Q.; Zhou, Z.; Zhuang, J.; Wang, X. Seed displacement, epitaxial synthesis of Rh/Pt bimetallic ultrathin nanowires for highly selective oxidizing ethanol to CO₂. *Chem. Mater.* **2010**, *22*, 2395–2402. [[CrossRef](#)]
11. Freitas, R.G.; Pereira, E.C.; Christensen, P.A. The selective oxidation of ethanol to CO₂ at Pt_{pc}/Ir/Pt metallic multilayer nanostructured electrodes. *Electrochem. Commun.* **2011**, *13*, 1147–1150. [[CrossRef](#)]
12. Zeller, G. Electrolytic oxidation of ethyl alcohol to acetic acid. *Trans. Electrochem. Soc.* **1947**, *92*, 335–342. [[CrossRef](#)]
13. Zhao, Y.; Yang, X.; Tian, J.; Wang, F.; Zhan, L. Methanol electro-oxidation on Ni@Pd core-shell nanoparticles supported on multi-walled carbon nanotubes in alkaline media. *Int. J. Hydrogen Energy* **2010**, *35*, 3249–3257. [[CrossRef](#)]
14. Zhou, W.J.; Song, S.Q.; Li, W.Z.; Sun, G.Q.; Xin, Q.; Kontou, S.; Poulianitis, K.; Tsiakaras, P. Pt-based anode catalysts for direct ethanol fuel cells. *Solid State Ionics* **2004**, *175*, 797–803. [[CrossRef](#)]
15. Lima, F.H.B.; Gonzalez, E.R. Ethanol electro-oxidation on carbon-supported Pt-Ru, Pt-Rh and Pt-Ru-Rh nanoparticles. *Electrochim. Acta* **2008**, *53*, 2963–2971. [[CrossRef](#)]
16. Zhao, Y.; Yang, X.; Zhan, L.; Ou, S.; Tian, J. High electrocatalytic activity of PtRu nanoparticles supported on starch-functionalized multi-walled carbon nanotubes for ethanol oxidation. *J. Mater. Chem.* **2011**, *21*, 4257–4263. [[CrossRef](#)]
17. Spendelow, J.S.; Wieckowski, A. Electrocatalysis of oxygen reduction and small alcohol oxidation in alkaline media. *Phys. Chem. Chem. Phys.* **2007**, *9*, 2654–2675. [[CrossRef](#)] [[PubMed](#)]
18. Shen, P.K.; Xu, C. Alcohol oxidation on nanocrystalline oxide Pd/C promoted electrocatalysts. *Electrochem. Commun.* **2006**, *8*, 184–188. [[CrossRef](#)]
19. Ma, L.; Chu, D.; Chen, R. Comparison of ethanol electro-oxidation on Pt/C and Pd/C catalysts in alkaline media. *Int. J. Hydrogen Energy* **2012**, *37*, 11185–11194. [[CrossRef](#)]
20. Rao, V.; Hariyanto; Cremers, C.; Stimming, U. Investigation of the ethanol electro-oxidation in alkaline membrane electrode assembly by differential electrochemical mass spectrometry. *Fuel Cells* **2007**, *7*, 417–423. [[CrossRef](#)]

21. Zheng, H.T.; Li, Y.; Chen, S.; Shen, P.K. Effect of support on the activity of Pd electrocatalyst for ethanol oxidation. *J. Power Sources* **2006**, *163*, 371–375. [[CrossRef](#)]
22. Ye, J.; Liu, J.; Xu, C.; Jiang, S.P.; Tong, Y. Electrooxidation of 2-propanol on Pt, Pd and Au in alkaline medium. *Electrochem. Commun.* **2007**, *9*, 2760–2763. [[CrossRef](#)]
23. Xu, C.; Shen, P.K.; Liu, Y. Ethanol electrooxidation on Pt/C and Pd/C catalysts promoted with oxide. *J. Power Sources* **2007**, *164*, 527–531. [[CrossRef](#)]
24. Nguyen, S.T.; Law, H.M.; Nguyen, H.T.; Kristian, N.; Wang, S.; Chan, S.H.; Wang, X. Enhancement effect of Ag for Pd/C towards the ethanol electro-oxidation in alkaline media. *Appl. Catal. B* **2009**, *91*, 507–515. [[CrossRef](#)]
25. Wang, W.; Zhang, J.; Yang, S.; Ding, B.; Song, X. Au@Pd core-shell nanobricks with concave structures and their catalysis of ethanol oxidation. *ChemSusChem* **2013**, *6*, 1945–1951. [[CrossRef](#)] [[PubMed](#)]
26. Shen, S.Y.; Zhao, T.S.; Xu, J.B.; Li, Y.S. Synthesis of PdNi catalysts for the oxidation of ethanol in alkaline direct ethanol fuel cells. *J. Power Sources* **2010**, *195*, 1001–1006. [[CrossRef](#)]
27. Wang, Y.; Zhao, Y.; Yin, J.; Liu, M.; Dong, Q.; Su, Y. Synthesis and electrocatalytic alcohol oxidation performance of Pd-Co bimetallic nanoparticles supported on graphene. *Int. J. Hydrogen Energy* **2014**, *39*, 1325–1335. [[CrossRef](#)]
28. Liu, J.; Zhou, H.; Wang, Q.; Zeng, F.; Kuang, Y. Reduced graphene oxide supported palladium-silver bimetallic nanoparticles for ethanol electro-oxidation in alkaline media. *J. Mater. Sci.* **2012**, *47*, 2188–2194. [[CrossRef](#)]
29. Zhang, Z.; Zhang, C.; Sun, J.; Kou, T.; Zhao, C. Ultrafine nanoporous Cu-Pd alloys with superior catalytic activities towards electro-oxidation of methanol and ethanol in alkaline media. *RSC Adv.* **2012**, *2*, 11820–11828. [[CrossRef](#)]
30. Wang, Y.; Shi, F.F.; Yang, Y.Y.; Cai, W.B. Carbon supported Pd-Ni-P nanoalloy as an efficient catalyst for ethanol electro-oxidation in alkaline media. *J. Power Sources* **2013**, *243*, 369–373. [[CrossRef](#)]
31. Mukherjee, P.; Roy, P.S.; Mandal, K.; Bhattacharjee, D.; Dasgupta, S.; Bhattacharya, S.K. Improved catalysis of room temperature synthesized Pd-Cu alloy nanoparticles for anodic oxidation of ethanol in alkaline media. *Electrochim. Acta* **2015**, *154*, 447–455. [[CrossRef](#)]
32. Dutta, A.; Datta, J. Energy efficient role of Ni/NiO in PdNi nano catalyst used in alkaline DEFC. *J. Mater. Chem. A* **2014**, *2*, 3237–3250. [[CrossRef](#)]
33. Rahim, M.A.A.; Hameed, R.M.A.; Khalil, M.W. Nickel as a catalyst for the electro-oxidation of methanol in alkaline medium. *J. Power Sources* **2004**, *134*, 160–169. [[CrossRef](#)]
34. Jiang, X.; Koizumi, N.; Guo, X.; Song, C. Bimetallic Pd-Cu catalysts for selective CO₂ hydrogenation to methanol. *Appl. Catal. B* **2015**, *170*, 173–185. [[CrossRef](#)]
35. Behmenyar, G.; Akin, A.N. Investigation of carbon supported Pd-Cu nanoparticles as anode catalysts for direct borohydride fuel cell. *J. Power Sources* **2014**, *249*, 239–246. [[CrossRef](#)]
36. Yang, L.; Hu, C.; Wang, J.; Yang, Z.; Cuo, Y.; Bai, Z.; Wang, K. Facile synthesis of hollow palladium/copper alloyed nanocubes for formic acid oxidation. *Chem. Commun.* **2011**, *47*, 8581–8583. [[CrossRef](#)] [[PubMed](#)]
37. Wang, F.; Zhao, K.; Zhang, H.; Dong, Y.; Wang, T.; He, D. Low temperature CO catalytic oxidation over supported Pd-Cu catalysts calcined at different temperatures. *Chem. Eng. J.* **2014**, *242*, 10–18. [[CrossRef](#)]
38. Ren, Y.; Zhang, S.; Lin, R.; Wei, X. Electro-catalytic performance of Pd decorated Cu nanowires catalyst for the methanol oxidation. *Int. J. Hydrogen Energy* **2015**, *40*, 2621–2630. [[CrossRef](#)]
39. Dong, Q.; Zhao, Y.; Han, X.; Wang, Y.; Liu, M.; Li, Y. Pd/Cu bimetallic nanoparticles supported on graphene nanosheets: Facile synthesis and application as novel electrocatalyst for ethanol oxidation in alkaline media. *Int. J. Hydrogen Energy* **2014**, *39*, 14669–14679. [[CrossRef](#)]
40. Na, H.Y.; Zhang, L.; Qiu, H.X.; Wu, T.; Chen, M.X.; Yang, N.; Li, L.Z.; Xing, F.B.; Gao, J.P. A two step method to synthesize palladium-copper nanoparticles on reduced graphene oxide and their extremely high electrocatalytic activity for the electrooxidation of methanol and ethanol. *J. Power Sources* **2015**, *288*, 160–167. [[CrossRef](#)]
41. Noborikawa, J.; Lau, J.; Ta, J.; Hu, S.; Scudiero, L.; Derakhshan, S.; Ha, S.; Haan, J.L. Palladium-copper electrocatalyst for promotion of oxidation of formate and ethanol in alkaline media. *Electrochim. Acta* **2014**, *137*, 654–660. [[CrossRef](#)]
42. Zhao, X.; Zhang, J.; Wang, L.; Liu, Z.; Chen, W. Pd_xCu_{100-x} networks: An active and durable electrocatalyst for ethanol oxidation in alkaline medium. *J. Mater. Chem. A* **2014**, *2*, 20933–20938. [[CrossRef](#)]

43. Mao, H.; Huang, T.; Yu, A. Surface palladium rich Cu_xPd_y /carbon catalysts for methanol and ethanol oxidation in alkaline media. *Electrochim. Acta* **2015**, *174*, 1–7. [[CrossRef](#)]
44. Zhu, F.; Ma, G.; Bai, Z.; Hang, R.; Tang, B.; Zhang, Z.; Wang, X. High activity of carbon nanotubes supported binary and ternary Pd-based catalysts for methanol, ethanol and formic acid electro-oxidation. *J. Power Sources* **2013**, *242*, 610–620. [[CrossRef](#)]
45. Liu, J.; Huang, Z.; Cai, K.; Zhang, H.; Lu, Z.; Li, T.; Zuo, Y.; Han, H. Clean synthesis of an economical 3D nanochain network of PdCu alloy with enhanced electrocatalytic performance towards ethanol oxidation. *Chem. Eur. J.* **2015**, *21*, 17779–17785. [[CrossRef](#)] [[PubMed](#)]
46. Mao, J.; Liu, Y.; Chen, Z.; Wang, D.; Li, Y. Bimetallic Pd–Cu nanocrystals and their tunable catalytic properties. *Chem. Commun.* **2014**, *50*, 4588–4591. [[CrossRef](#)] [[PubMed](#)]
47. Xu, C.; Liu, Y.; Wang, J.; Geng, H.; Qiu, H. Nanoporous PdCu alloy for formic acid electro-oxidation. *J. Power Sources* **2012**, *199*, 124–131. [[CrossRef](#)]
48. Zhang, J.; Ma, J.; Wan, Y.; Jiang, J.; Zhao, X.S. Dendritic Pt–Cu bimetallic nanocrystals with a high electrocatalytic activity toward methanol oxidation. *Mater. Chem. Phys.* **2012**, *132*, 244–247. [[CrossRef](#)]
49. Zhang, X.; Hu, Y.; Zhu, D.; Xie, A.; Shen, Y. A novel porous CuO nanorod/rGO composite as a high stability anode material for lithium-ion batteries. *Ceram. Int.* **2016**, *42*, 1833–1839. [[CrossRef](#)]
50. Hu, Z.; Liu, H. Three-dimensional CuO microflowers as anode materials for Li-ion batteries. *Ceram. Int.* **2015**, *41*, 8257–8260. [[CrossRef](#)]
51. Wang, J.; Zhao, F.; Cao, J.; Liu, Y.; Wang, B. Enhanced electrochemical performance of Cu_2O -modified $\text{Li}_4\text{Ti}_5\text{O}_{12}$ anode material for lithium-ion batteries. *Ionics* **2015**, *21*, 2155–2160. [[CrossRef](#)]
52. Pan, L.; Tang, J.; Wang, F. Facile synthesis of nanoscaled $\alpha\text{-Fe}_2\text{O}_3$, CuO and CuO/ Fe_2O_3 hybrid oxides and their electrocatalytic and photocatalytic properties. *Cent. Eur. J. Chem.* **2013**, *11*, 763–773. [[CrossRef](#)]
53. Gusain, R.; Kumar, P.; Sharma, O.P.; Jain, S.L.; Khatri, O.P. Reduced graphene oxide–CuO nanocomposites for photocatalytic conversion of CO_2 into methanol under visible light irradiation. *Appl. Catal. B* **2016**, *181*, 352–362. [[CrossRef](#)]
54. Yue, G.H.; Zhang, Y.; Zhang, X.Q.; Wang, C.G.; Zhao, Y.C.; Peng, D.L. Synthesis of Cu_2O mesocrystal and its application in photocatalysis. *Appl. Phys. A* **2015**, *118*, 763–767. [[CrossRef](#)]
55. Zhao, X.; Wang, P.; Yan, Z.; Ren, N. Room temperature photoluminescence properties of CuO nanowire arrays. *Opt. Mater.* **2015**, *42*, 544–547. [[CrossRef](#)]
56. Garuthara, R.; Siripala, W. Photoluminescence characterization of polycrystalline n-type Cu_2O films. *J. Lumin.* **2006**, *121*, 173–178. [[CrossRef](#)]
57. Fan, Y.; Liu, P.F.; Yang, Z.J. CuO nanoparticles supported on carbon microspheres as electrode material for supercapacitors. *Ionics* **2015**, *21*, 185–190. [[CrossRef](#)]
58. Park, H.; Han, T.H. Facile hybridization of graphene oxide and Cu_2O for high-performance electrochemical supercapacitors. *Macromol. Res.* **2014**, *22*, 809–812. [[CrossRef](#)]
59. Luo, D.; Li, Y.; Liu, J.; Feng, H.; Qian, D.; Peng, S.; Jiang, J.; Liu, Y. One-step solution-phase synthesis of a novel RGO– Cu_2O – TiO_2 ternary nanocomposite with excellent cycling stability for supercapacitors. *J. Alloys Compd.* **2013**, *581*, 303–307. [[CrossRef](#)]
60. Sharma, J.K.; Akhtar, M.S.; Ameen, S.; Srivastava, P.; Singh, G. Green synthesis of CuO nanoparticles with leaf extract of *Calotropis gigantea* and its dye-sensitized solar cells applications. *J. Alloys Compd.* **2015**, *632*, 321–325. [[CrossRef](#)]
61. Soundaram, N.; Chandramohan, R.; Valanarasu, S.; Thomas, R.; Kathalingam, A. Studies on SILAR deposited Cu_2O and ZnO films for solar cell applications. *J. Mater. Sci. Mater. Electron.* **2015**, *26*, 5030–5036. [[CrossRef](#)]
62. Katoch, A.; Choi, S.W.; Kim, J.H.; Lee, J.H.; Lee, J.S.; Kim, S.S. Importance of the nanograin size on the H_2S -sensing properties of ZnO–CuO composite nanofibers. *Sens. Actuators B* **2015**, *214*, 111–116. [[CrossRef](#)]
63. Zhang, J.; Liu, J.; Peng, Q.; Wang, X.; Li, Y. Nearly monodisperse Cu_2O and CuO nanospheres: Preparation and applications for sensitive gas sensors. *Chem. Mater.* **2006**, *18*, 867–871. [[CrossRef](#)]
64. Zhang, J.; Ma, J.; Zhang, S.; Wang, W.; Chen, Z. A highly sensitive nonenzymatic glucose sensor based on CuO nanoparticles decorated carbon spheres. *Sens. Actuators B* **2015**, *211*, 385–391. [[CrossRef](#)]
65. Gao, P.; Liu, D. Petal-like CuO nanostructures prepared by a simple wet chemical method, and their application to non-enzymatic amperometric determination of hydrogen peroxide. *Microchim. Acta* **2015**, *182*, 1231–1239. [[CrossRef](#)]

66. Li, Y.; Zhong, Y.; Zhang, Y.; Weng, W.; Li, S. Carbon quantum dots/octahedral Cu₂O nanocomposites for non-enzymatic glucose and hydrogen peroxide amperometric sensor. *Sens. Actuators B* **2015**, *206*, 735–743. [[CrossRef](#)]
67. Zhao, Y.; Song, X.; Yin, Z.; Song, Q. One-step self-assembled synthesis of CuO with tunable hierarchical structures and their electrocatalytic properties for nitrite oxidation in aqueous media. *J. Colloid Interface Sci.* **2013**, *396*, 29–38. [[CrossRef](#)] [[PubMed](#)]
68. Ma, Y.; Li, H.; Wang, R.; Wang, H.; Lv, W.; Ji, S. Ultrathin willow-like CuO nanoflakes as an efficient catalyst for electro-oxidation of hydrazine. *J. Power Sources* **2015**, *289*, 22–25.
69. Liu, X.; Cui, S.; Sun, Z.; Du, P. Copper oxide nanomaterials synthesized from simple copper salts as active catalysts for electrocatalytic water oxidation. *Electrochim. Acta* **2015**, *160*, 202–208. [[CrossRef](#)]
70. Yang, Y.J.; Li, W.; Chen, X. Highly enhanced electrocatalytic oxidation of glucose on Cu(OH)₂/CuO nanotube arrays modified copper electrode. *J. Solid State Electrochem.* **2012**, *16*, 2877–2881. [[CrossRef](#)]
71. Wang, C.; Liu, J.; Huang, X.; Wang, H.; Zheng, Y.; Lin, L.; Wang, S.; Chen, S.; Jin, Y. Cupric oxide nanowires assembled by nanoparticles *in situ* with enhancing electrocatalytic oxidation of ascorbic acid. *Appl. Surf. Sci.* **2014**, *292*, 291–296. [[CrossRef](#)]
72. Yan, X.Y.; Tong, X.L.; Zhang, Y.F.; Han, X.D.; Wang, Y.Y.; Jin, G.Q.; Qin, Y.; Guo, X.Y. Cuprous oxide nanoparticles dispersed on reduced graphene oxide as an efficient electrocatalyst for oxygen reduction reaction. *Chem. Commun.* **2012**, *48*, 1892–1894. [[CrossRef](#)] [[PubMed](#)]
73. Felix, S.; Kollu, P.; Raghupathy, B.P.C.; Jeong, S.K.; Grace, A.N. Electrocatalytic activity of Cu₂O nanocubes based electrode for glucose oxidation. *J. Chem. Sci.* **2014**, *126*, 25–32. [[CrossRef](#)]
74. Rostami, H.; Rostami, A.A.; Omrani, A. An electrochemical method to prepare of Pd/Cu₂O/MWCNT nanostructure as an anode electrocatalyst for alkaline direct ethanol fuel cells. *Electrochim. Acta* **2016**, *194*, 431–440. [[CrossRef](#)]
75. Cheng, W.H. Reaction and XRD studies on Cu based methanol decomposition catalysts: Role of constituents and development of high-activity multicomponent catalysts. *Appl. Catal. A* **1995**, *130*, 13–30. [[CrossRef](#)]
76. Sieben, J.M.; Alvarez, A.E.; Comignani, V.; Duarte, M.M.E. Methanol and ethanol oxidation on carbon supported nanostructured Cu core Pt–Pd shell electrocatalysts synthesized via redox displacement. *Int. J. Hydrogen Energy* **2014**, *39*, 11547–11556. [[CrossRef](#)]
77. Holzwarth, U.; Gibson, N. The Scherrer equation *versus* the ‘Debye-Scherrer equation’. *Nat. Nanotechnol.* **2011**, *6*, 534–534. [[CrossRef](#)] [[PubMed](#)]
78. Liu, Z.; Lee, J.Y.; Chen, W.; Han, M.; Gan, L.M. Physical and electrochemical characterizations of microwave-assisted polyol preparation of carbon-supported PtRu nanoparticles. *Langmuir* **2004**, *20*, 181–187. [[CrossRef](#)] [[PubMed](#)]
79. Lu, Y.; Jiang, Y.; Wu, H.; Chen, W. Nano-PtPd cubes on graphene exhibit enhanced activity and durability in methanol electrooxidation after CO stripping-cleaning. *J. Phys. Chem. C* **2013**, *117*, 2926–2938. [[CrossRef](#)]
80. Wen, W.; Li, C.; Li, W.; Tian, Y. Carbon-supported Pd–Cr electrocatalysts for the electrooxidation of formic acid that demonstrate high activity and stability. *Electrochim. Acta* **2013**, *109*, 201–206. [[CrossRef](#)]
81. Kim, K.S.; Gossmann, A.F.; Winograd, N. X-ray photoelectron spectroscopic studies of palladium oxides and the palladium-oxygen electrode. *Anal. Chem.* **1974**, *46*, 197–200. [[CrossRef](#)]
82. Ding, K.; Li, Y.; Zhao, Y.; Liu, L.; Gu, H.; Liu, L.; Qiu, S.; He, C.; Liu, J.; Wang, Q.; *et al.* Dry-grinding synthesized multi-walled carbon nanotubes supported PdO catalyst for ethanol oxidation reaction. *Electrochim. Acta* **2014**, *149*, 186–192. [[CrossRef](#)]
83. Mao, H.; Wang, L.; Zhu, P.; Xu, Q.; Li, Q. Carbon-supported PdSn–SnO₂ catalyst for ethanol electro-oxidation in alkaline media. *Int. J. Hydrogen Energy* **2014**, *39*, 17583–17588. [[CrossRef](#)]
84. Du, C.; Chen, M.; Wang, W.; Yin, G. Nanoporous PdNi alloy nanowires as highly active catalysts for the electro-oxidation of formic acid. *ACS Appl. Mater. Interfaces* **2010**, *3*, 105–109. [[CrossRef](#)] [[PubMed](#)]
85. Zhang, L.; Wan, L.; Ma, Y.; Chen, Y.; Zhou, Y.; Tang, Y.; Lu, T. Crystalline palladium-cobalt alloy nanoassemblies with enhanced activity and stability for the formic acid oxidation reaction. *Appl. Catal. B* **2013**, *138*, 229–235. [[CrossRef](#)]
86. Yu, B.; Wen, W.; Li, W.; Yang, Y.; Hou, D.; Liu, C. Fabrication of high performance carbon-supported ternary Pd–Cu–Fe electrocatalysts for formic acid electrooxidation via partly galvanic sacrifice of tunable binary Cu–Fe alloy templates. *Electrochim. Acta* **2016**, *196*, 223–230. [[CrossRef](#)]

87. Yang, G.; Chen, Y.; Zhou, Y.; Tang, Y.; Lu, T. Preparation of carbon supported Pd-P catalyst with high content of element phosphorus and its electrocatalytic performance for formic acid oxidation. *Electrochem. Commun.* **2010**, *12*, 492–495. [[CrossRef](#)]
88. Wakisaka, M.; Mitsui, S.; Hirose, Y.; Kawashima, K.; Uchida, H.; Watanabe, M. Electronic structures of Pt-Co and Pt-Ru alloys for CO-tolerant anode catalysts in polymer electrolyte fuel cells studied by EC-XPS. *J. Phys. Chem. B* **2006**, *110*, 23489–23496. [[CrossRef](#)] [[PubMed](#)]
89. Paixão, T.R.L.C.; Bertotti, M. Development of a breath alcohol sensor using a copper electrode in an alkaline medium. *J. Electroanal. Chem.* **2004**, *571*, 101–109. [[CrossRef](#)]
90. Maiyalagan, T.; Scott, K. Performance of carbon nanofiber supported Pd-Ni catalysts for electro-oxidation of ethanol in alkaline medium. *J. Power Sources* **2010**, *195*, 5246–5251. [[CrossRef](#)]
91. Reyter, D.; Bélanger, D.; Roué, L. Elaboration of Cu-Pd films by coelectrodeposition: Application to nitrate electroreduction. *J. Phys. Chem. C* **2008**, *113*, 290–297. [[CrossRef](#)]
92. Liang, Z.X.; Zhao, T.S.; Xu, J.B.; Zhu, L.D. Mechanism study of the ethanol oxidation reaction on palladium in alkaline media. *Electrochim. Acta* **2009**, *54*, 2203–2208. [[CrossRef](#)]
93. Qin, Y.H.; Yang, H.H.; Zhang, X.S.; Li, P.; Ma, C.A. Effect of carbon nanofibers microstructure on electrocatalytic activities of Pd electrocatalysts for ethanol oxidation in alkaline medium. *Int. J. Hydrogen Energy* **2010**, *35*, 7667–7674. [[CrossRef](#)]
94. Li, W.; Fan, F.R.F.; Bard, A.J. The application of scanning electrochemical microscopy to the discovery of Pd-W electrocatalysts for the oxygen reduction reaction that demonstrate high activity, stability, and methanol tolerance. *J. Solid State Electrochem.* **2012**, *16*, 2563–2568. [[CrossRef](#)]



© 2016 by the authors; licensee MDPI, Basel, Switzerland. This article is an open access article distributed under the terms and conditions of the Creative Commons Attribution (CC-BY) license (<http://creativecommons.org/licenses/by/4.0/>).